Journal of the Korean Physical Society, Vol. 40, No. 4, April 2002, pp. 577∼583

Comprehensive Characterization and Modeling of the Abnormal Gate Leakage Current in Pseudomorphic HEMTs

S. D. Cho, H. T. Kim, S. J. Song, H. C. Kim, Y. C. Kim, S. K. Kim, D. J. Kim and D. M. Kim*
School of Electrical Engineering, Kookmin University, Seoul 136-702

(Received 11 February 2001, in final form 6 March 2002)

Systematic characterization and qualitative modeling of the abnormal gate leakage current in GaAs-based commercial pseudomorphic HEMTs with gate lengths of 0.2 μm are reported with a unique resonant tunneling mechanism for the first time. In the modeling of the abnormal I-V characteristics, all possible physical mechanisms are included for a proper description and the characteristics are divided into 4 different voltage regions. They consist of the normal reverse leakage current, the negative hump due to impact ionization, the abnormal positive hump induced by the resonant tunneling, and the forward conduction that results in a negative differential resistance (NDR) for the drain current. In particular, the abnormal positive and negative humps in the gate current and the negative differential resistance (NDR) in the drain current have been investigated, and physical models are provided. Experimental verification has been also provided for the abnormal gate leakage current that occurs under a high drain bias (V_{DS}>2.3 V) with a forward gate bias (0.2<V_{GS}<0.6) due to the formation of hybrid-excited states across the InGaAs channel and the AlGaAs donor layer. These results will provide a comprehensive interpretations of the abnormal positive humps in I_G caused by resonant-tunneling and of the NDR of the drain current due to a field-assisted tunneling real-space transfer caused by hot channel electrons. This work is also expected to be helpful for implementing more robust and reliable pseudomorphic HEMT-based MMICs and MIMICs.

PACS numbers: 81.05.Ea
Keywords: PHEMT, Leakage current

I. INTRODUCTION

Since the pseudomorphic high-electron mobility transistor (PHEMT) was introduced in 1986, it has been known that PHEMT is one of the most commercially promising devices for ultra-high frequency and high-speed signal processing circuits and systems. High performance in the devices requires a large saturation current (I_{DSS}), a large transconductance (g_m), a higher current gain cut-off frequency (f_T), and a superior minimum noise figure (NF_{min}) defined by

$$g_m(max) = q\mu_n N_D a \left(\frac{W}{L}\right), \quad (1)$$

$$f_T(max) = \frac{g_m(max)}{2\pi C_G(min)} = \frac{q\mu_n N_D}{2\pi\epsilon_1} a^2 \left[\frac{1}{L^2}\right], \quad (2)$$

$$NF_{min} = 1 + k_f(f/f_T)\left[g_m(R_s + R_g)\right]^{1/2}, \quad (3)$$

respectively, and scaling of the gate length (L) to the deep sub-micrometer range (typically lower than 0.25 μm) is one of best ways to achieve a high transconductance and cut-off frequency [1,2].

However, the gate leakage characteristics and the breakdown effects of the devices unfortunately limit the design and fabrication technology [3, 4]. Therefore, it is essential that further improvements, high reliability, good noise performance, and excellent stability of the electrical characteristics, be made for reliable operation of PHEMTs in a number of interesting applications, such as wireless and optical communication systems. Several papers have been published on various reliability issues, when PHEMTs are biased at high drain voltages, related to the long-term stability of short channel devices [5, 6]. Such phenomena are caused by the presence of a large electric field in the high-mobility channel and a heterobarrier between the InGaAs channel and the AlGaAs donor layer. These physical effects will generally generate additional trap levels due to hot carrier damage or filling/emitting electrons in existing trap levels under the gate or at the surface/Schottky interfacial layers. As a result of the traps, DC and RF characteristics may show a degradation in gain, a shift in the threshold voltage, and breakdown walkout, thereby affecting the performance of circuits and systems with PHEMTs [5]. These degradations are attributed to surface- or deep-

*E-mail: dmkim@kookmin.ac.kr; Fax : +82-2-910-4449

trap-related mechanisms. Also, the negative differential resistance (NDR) phenomenon in the drain-source current has been observed in PHEMTs and is associated with thermionic emission and tunneling from the high-mobility InGaAs channel to the gate electrode through the low-mobility AlGaAs donor layer at a large forward gate bias [7]. Recently, this region has been implemented successfully for various analog and digital circuit applications with PHEMTs. Therefore, the gate leakage currents must be analyzed by using accurate numerical and theoretical modeling over the entire bias region in order to implement robust and reliable implementation of MMICs and MIMICs with PHEMTs.

In this work, we investigate the abnormal electrical characteristics of gate leakage currents, which can be divided into four regions: normal reverse leakage currnets, negative hump currents, abnormal positive hump gate currents, and forward Schottky currents. This work discusses comprehensive physical mechanisms for the abnormal gate leakage currents and can be used to predict potential symptoms and methods for implementing reliable PHEMTs. The mechanisms for generating the gate leakage current in each region consist of impact ionization, thermionic emission, field-assisted tunneling, resonant tunneling, and real-space transfer. Especially, as the published works generally have focused on the hot-electron effect due to impact-ionization [8], there has been no indication of a possible analysis of the abnormal positive hump of gate leakage currents. We expand on and make more thorough presentations of physical models for gate leakage current generation based on resonant tunneling and field-assisted real-space transfer.

II. DEVICES AND EXPERIMENTAL DISCUSSION

Commercial pseudomorphic HEMTs, which are suitable for applications in ultra-sensitive low-noise amplifiers up to 12 GHz, were employed for this work. The devices had a 0.2-μm gate length with a total gate width=200 μm and were packaged in low-parasitic, surface-mountable ceramic packages. Proven gold-based-metalization systems and nitride passivation assured reliable devices.

Tested devices had a drain saturation current of I_{DSS}~30 mA (measured at V_{DS}=1.5 V, V_{GS}=0 V) and a transconductance of g_m~55 mS (measured at V_{DS}=1.5 V, V_{GS}=0 V). Typical values of the minimum noise figure and the associated gain at f=12 GHz, reported on the datasheets, were 0.5 dB and 12 dB, respectively, at V_{DS}=1.5 V, V_{GS}=0 V. The measured results were obtained with an HP4145B semiconductor parameter analyzer controlled by a personal computer. Figures 1(a) and 1(b) show the I versus V characteristics ($I_{DS}-V_{DS}$, $I_{DS}-V_{GS}$) measured for typical 0.2 μm×200 μm PHEMTs at room temperatures and Fig. 2 shows the measured transconductance as a function of the gate-source voltage.

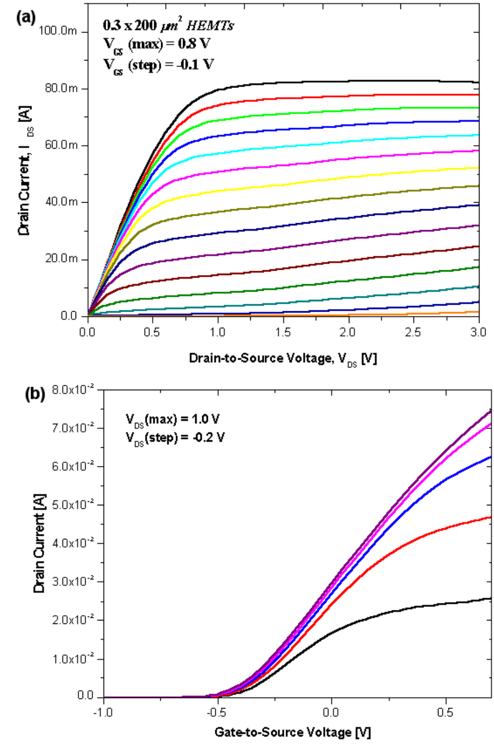

Fig. 1. (a) Drain current I_D as a function of V_{DS} and V_{GS} ($V_{GS,max}$=0.8~−0.6 V, step=−0.1 V). (b) Drain current I_D as a function of V_{GS} at different values of V_{DS} ($V_{DS,max}$=1.0~0.2 V, step=−0.2 V).

Figure 3 shows the abnormal gate leakage currents, I_G, as a function of V_{GS} for increasing V_{DS}($V_{DS,max}$=3.8 V, step −0.2 V) measured at room temperature. For negative V_{GS}(<−0.54 V), the gate currents can be considered as typical gate-drain Schottky diode reverse currents. Due to the high electric field in the gate-drain

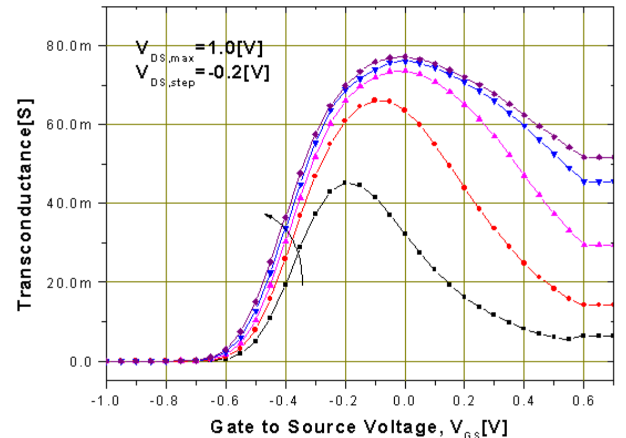

Fig. 2. Transconductance g_m as a function of V_{GS} at different values of V_{DS}.

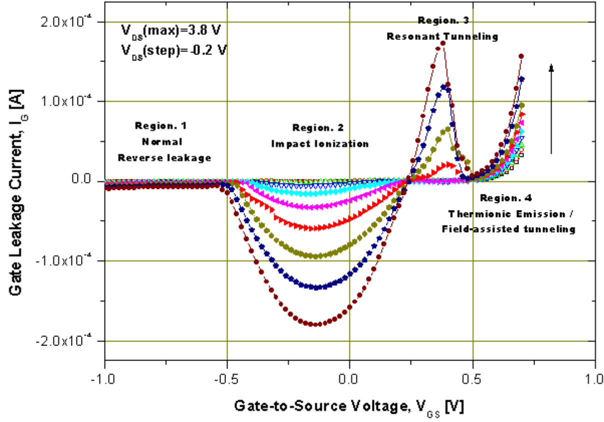

Fig. 3. Abnormal gate leakage currents with four different regions defined by considering physical mechanism: Region 1: the normal reverse leakage, Region 2: the negative hump, Region 3: the abnormal positive hump, and Region 4: the forward Schottky conduction.

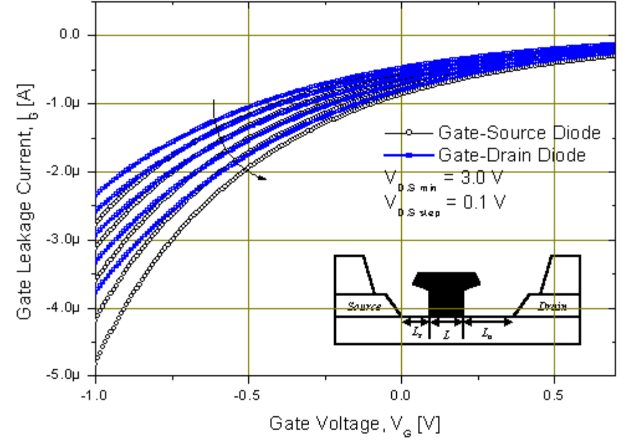

Fig. 4. Reverse gate leakage currents in gate-source diode and gate-drain diode as functions of V_{GS}.

region as the device is biased at high V_{DS}, the gate leakage currents in the PHEMTs show anomalous negative and positive bell-shaped behaviors as a function of V_{GS}. While the negative hump of the gate currents is believed to be the cause of the significant hot-electron phenomena due to the holes generated by the impact ionization, the positive hump of the gate current can't be explained only by the hot-electron mechanism in the drain region. This new phenomenon requires a theoretical concept that proves itself in the metal-AlGaAs-InGaAs structure dependent upon V_{GD}, as well as up on V_{DS}. When the forward gate bias was increased beyond V_{GS}=0.6 V, a forward gate current, which is associated with the negative differential resistance (NDR) phenomenon, was also observed in the PHEMTs. At a high V_{DS} bias, the gate current of this region can not be explained only by the thermionic emission process.

In order to identify the physical mechanisms related to the abnormal positive hump and the forward conduction of the gate leakage currents in PHEMTs, we performed a number of measurements to guarantee the confidence of the abnormal behaviors. In the next section, we give a description of the gate current in each region of the current-voltage characteristics for PHEMTs.

III. ANALYSIS OF THE ABNORMAL GATE LEAKAGE CURRENT

Region 1: In this region, as shown in Fig. 3, the generation current with impact ionization in the depletion region under the gate is the dominant current mechanism. The gate current in Region 1 is the same as that in reverse-biased diodes and is mainly determined by the inherent Schottky barrier height and the depletion width under a large reverse bias. Therefore, the gate leakage current of this region can be used to estimate the input gate noise performance and the breakdown effect and it predicts a higher input gate noise and a lower breakdown voltage due to the high reverse leakage current. In particular, numerous theoretical and experimental studies of breakdown in PHEMTs have appealed to impact ionization, tunneling, and thermionic field emission [9]. Due to these limiting factors, the design aspect of devices features an asymmetric double recess structures [10]. The asymmetry of the test device is obvious in Fig. 4, which compares the behavior of source-gate and drain-gate diodes in a two-terminal configuration. At low reverse bias, the drain-gate and the source-gate diodes behave identically while at higher reverse biases, the source-gate diode exhibits a significantly higher leakage current than the drain-gate diode, as the depletion region extends into the asymmetrically wide recess structure.

In order to understand the breakdown mechanism of the reverse leakage current in this device, we performed two- and three-terminal measurements as functions of V_{DS} and V_{GS}. Figure 5(a) shows the measured off-state breakdown voltages in both the two- and the three-terminal configurations. The two-terminal off-state breakdown voltages (BV_{DG} and BV_{SG}) were measured between 8 and 10 V while the three-terminal off-state breakdown voltages were measured between 6 and 8 V. When the drain-source voltage, V_{DS}, was increased for identical leakage current level, the drain-gate voltage was measured between 2.8 and 3.6 V, as shown Fig. 5(b). It is thought that the breakdown voltage is determined by the avalanche multiplication effect due to impact ionization.

Region 2: In this region, as shown Fig. 3, a bell-shaped negative hump in the gate current is observed for the test device. Such behavior has been reported to be due to a hot-electron effect caused by impact ionization. In this region, the gate current is proportional to $\alpha_n \cdot L_{eff}$ and to I_D, where α_n is the electron impact-ionization coefficient

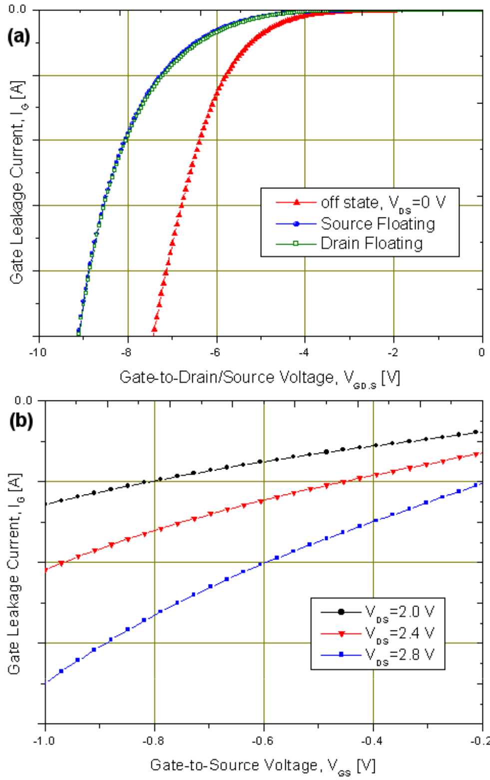

Fig. 5. Two- and three-terminal gate leakage currents measured as functions of V_{DS} and the V_{GS} bias: (a) two-terminal off-state breakdown voltages (8∼10 V), three-terminal off-state breakdown voltage (6∼8 V), and (b) the drain-gate voltage measured between 2.8 and 3.6 V for the same leakage current level.

of the channel and L_{eff} is the extension of the channel region where the impact ionization takes place:

$$|I_G| = I_D \alpha_N \cdot L_{ff} \cong I_D L_{ff} \exp\left(\frac{1}{E}\right) \quad (4)$$

and E is the longitudinal electric field in the L_{eff} region. According to Eq. (4), when the electric field in the L_{eff} region of the channel increases, energetic electrons due to impact ionization may provide valence-band electrons with sufficient energy to leap into the conduction band, leaving a hole behind. The generated electron-hole pairs are split and accelerated in the electric field at the L_{eff} region in channel. Although the electrons easily reach the nearby drain, some of holes flowing toward the source may overcome the valence-band discontinuity (ΔE_V) and experience field-assisted real-space transfer into the barrier layer, being consecutively collected by the gate electrode and forming a gate current. Similar to the gate and substrate currents based on the hot-carrier effect in MOSFETs, the gate current curve in this region has a bell shape. It is important that the gate current is a strong function of both the longitudinal field in the channel and the transverse field in the AlGaAs donor layers which are predominantly controlled

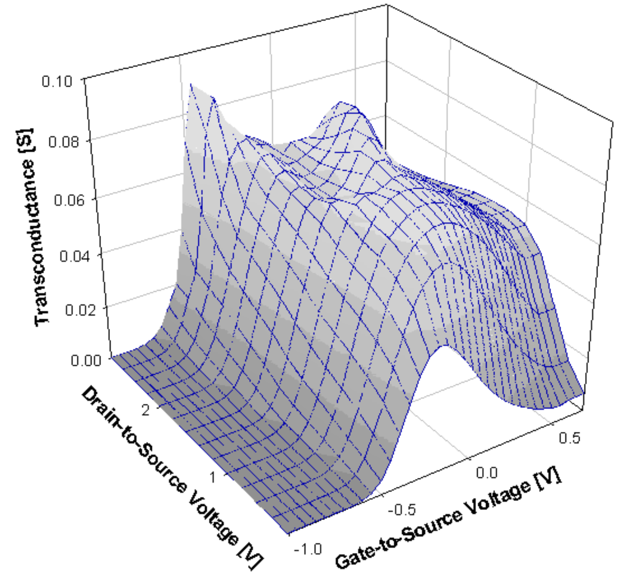

Fig. 6. Degradation of the transconductance g_m as a function of V_{GS} at high V_{DS}.

by V_{DS} and V_{GS}. When V_{GS} is low and V_{DS} is high, although the transverse electric field may be large, only a few electrons reside in the channel. As V_{GS} is raised, the electron population in the channel increases; therefore, the channel electron concentration grows causing an enhancement of the gate leakage due to the impact ionization. If V_{GS} continues to increase, however, the peak longitudinal field at the drain end of the channel is reduced so that the negative gate leakage reaches a maximum and then starts to decrease. Figure 6 shows the degradation of the transconductance caused by the negative hump in the gate current at high drain biases.

Region 3: For a possible explanation of the abnormal positive hump in Region 3, as shown Fig. 3, we incorporate resonant tunneling into the hot-electron effect to obtain the abnormal positive hump in the gate leakage current of PHEMTs at room temperature. Resonant tunneling is a quantum-mechanical process that manifests itself in particles tunneling through a sequence of classically forbidden regions sandwiching a classically allowed region [11]. The forbidden regions must be thin enough so that particles can tunnel through, and the allowed region should be thick enough to allow the existence of eigen-energy states. These conditions correlate with the metal-AlGaAs-InGaAs structure in HEMTs when the gate-source is biased between the pinch-off voltage and the forward-conduction onset-voltage. Figure 7 shows the three distinct regions of current-voltage behavior with the band diagrams in the conventional resonant tunneling diodes (RTD) [11]. The peak currents through such coupled barriers occur when the Fermi level is at the same energy as the bound-state energy level.

Resonant tunneling in PHEMTs can occur when enough hot electrons caused by impact ionization are

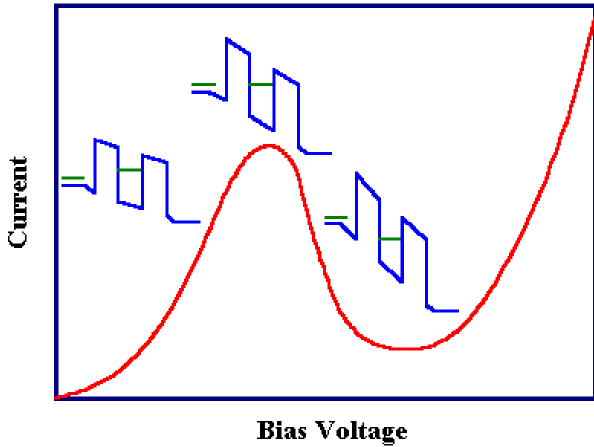

Fig. 7. Three distinct regions of the current-voltage behavior with a schematic energy band diagram.

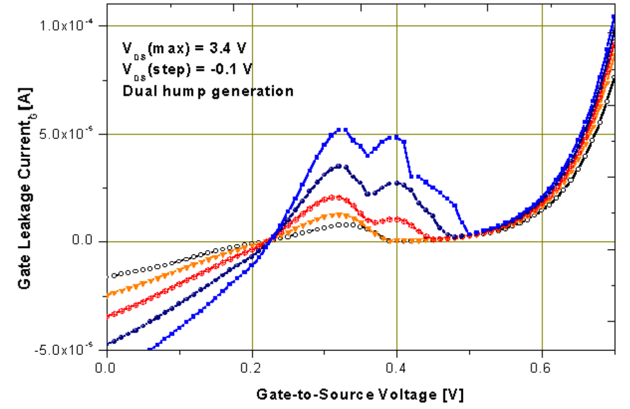

Fig. 9. Dual hump of abnormal gate leakage currents due to resonant tunneling measured at $V_{GS,max}$=3.4 V and $V_{GS,step}$=−0.1 V.

excited to two-dimensional quantized states in the high-mobility InGaAs channel and which are hybridized with two-dimensional quantized states in the high-gap low-mobility AlGaAs donor layer [12]. We focus on the simultaneous conditions of sufficient hot-electron occupation of the quantized states in the InGaAs channel and hybridization between the lowest quantized AlGaAs level and the first/second quantized InGaAs levels. The hybrization is a sensitive function of the gate voltage while the hot-electron occupation of quantized states is controlled by the drain-to-source voltage. The energy-band diagrams for a metal-AlGaAs-InGaAs structure are illustrated in Figs. 8(a)∼8(d). A large value of V_{DS} heats up the electrons in the InGaAs channel and increases the occupation by hot electrons of higher quantized energy states (see Fig. 8(a)). In addition, increasing V_{GS} (reducing V_{GD} at the drain end), which is proportional to creating additional localized states in the AlGaAs layer and increasing the quasi-Fermi level, causes hybridization between the lowest quantized AlGaAs level and the first quantized InGaAs level (see Fig. 8(b)). If we keep pushing V_{GS} up, the lowest quantized AlGaAs level crosses/overlaps the second quantized InGaAs level so that they form a hybrid (see Fig. 8(c)). Then, electrons tunnel through the heterobarrier from the InGaAs channel to the AlGaAs donor layer. On increasing V_{GS}, the occupation by electrons of the lowest quantized level in the AlGaAs layer may be reduced due to the difference between the quasi-Fermi level and the conduction band edge (see Fig. 8(d)). Figure 9 shows the measured dual hump of abnormal gate currents for hot-electron conditions. Because the states in the channel localize over a small energy difference, the dual hump of the abnormal gate current caused by resonant tunneling can be observed over a small voltage range.

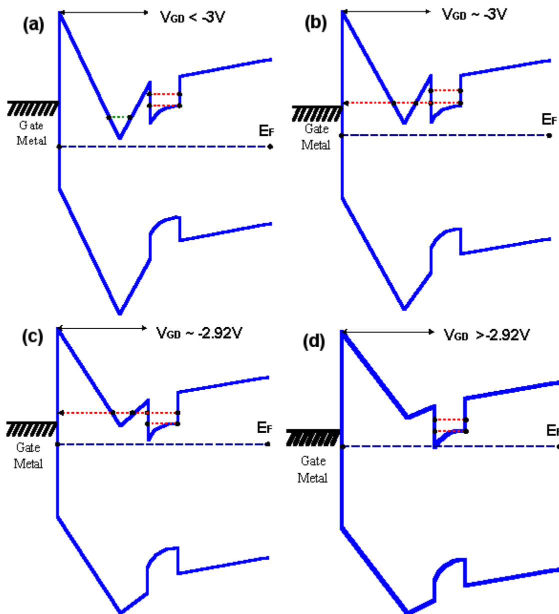

Fig. 8. Energy band diagram of the DUT: (a) the occupation by hot electrons of quantized energy states due to the application of a high V_{DS}, (b) The onset of resonant tunneling between the quantized AlGaAs level and the first quantized InGaAs level, (c) The onset of resonant tunneling across the second quantized InGaAs level, and (d) The reduction of electrons on the lowest quantized level in the AlGaAs layer.

Region 4: Finally, in Region 4, there are two physical mechanisms associated with the forward gate current. The forward conduction onset starts up at V_{GS}=0.7 V with V_{DS}=0 V when the gate-channel diodes are forward biased. In this bias condition, the channel electron concentration increases and results in an elevated gate leakage due to the thermionic emission (TE). As V_{DS} is increased, however, the quasi-Fermi level will be far below the conduction band at the drain end of the channel, decreasing the gate leakage current due to TE, as shown Fig. 10. When V_{DS} is higher than V_{GS}=0.7 V, although the gate leakage current due to TE shrinks because the region biased below V_{GS}=0.7 V by TE is extended along

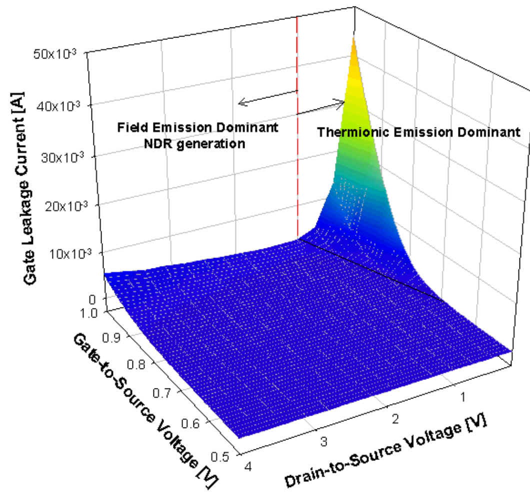

Fig. 10. Forward Schottky gate leakage currents as functions of VGS and VDS for VDS<1 V. Thermionic emission is dominant when V_{DS}>1 V. When field emission is dominant a NDR is generated.

the quantum-well channel toward the source from the drain end, the gate leakage current starts to go up at the drain end of the channel. Therefore, if V_{DS} is continually raised, the two-dimensional electrons drift along the quantum-well channel from the source toward the drain, and some of them acquire large enough energies to be real-space transferred into the AlGaAs layer through the undoped spacer layer by field-assisted tunneling real-space transfer (FTRST). This behavior can be explained qualitatively by a real-space transfer mechanism due to the hot-carrier tunneling under a high drain field. Then, the gate leakage current increases again, as shown Fig. 10.

With these considerations, the distinction between the forward conduction gate currents due to TE and FTRST

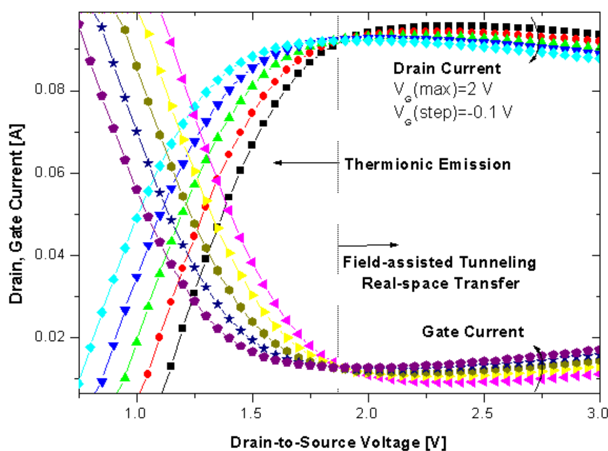

Fig. 11. Forward gate currents correlate to the corresponding drain current, resulting in the negative differential resistance.

becomes more understandable. This increase of the gate leakage current is correlated to a corresponding decrease in the drain current, resulting in a negative differential resistance (NDR). Figure 11 shows the relation between the drain current and the gate current. In this new proposed model, NDR is FTRST induced when enough hot electrons are exited to the drain end of the channel. This result indicates that PHEMTs can be operated in a new mode under high-bias conditions as gate- and drain-controlled NDR-type microwave amplifiers or oscillators [13,14].

IV. CONCLUSION

We have used experimental data to provide a comprehensive characterization of the physical mechanisms in the abnormal gate leakage current. We also proposed unique and extensive qualitative models for the abnormal current-voltage characteristics in PHEMTs. The physical mechanisms for the gate current generation in each region could be classified as a normal reverse leakage, a hot-electron effect due to impact ionization, resonant tunneling, and field-assisted tunneling real-space transfer. Especially, for the first time as far as we know, we incorporated the concept of resonant tunneling into the hot-electron effect to explain the abnormal positive humps in the gate leakage current. We also provided direct evidence for the dual hump characteristics to confirm the resonant-tunneling mechanism. With the considerations in this paper, an interpretation of the abnormal positive humps in gate leakage current caused by resonant tunneling and the distinction between the forward conduction gate currents due to the thermionic emission (TE) and field-assisted tunneling real-space transfer (FTRST) become more understandable.

ACKNOWLEDGMENTS

This work was supported by Korea Research Foundation Grant (KRF-2001-041-E00166).

REFERENCES

[1] H.-S. Yoon, J. Lee, B.-S. Park, C.-E. Yun and C.-S. Park, J. Korean Phys. Soc. **33**, 741 (1998).
[2] J.-H. Lee, H.-T. Choi, C.-W. Lee, H.-S. Yoon, B.-S. Park and C.-S. Park, J. Korean Phys. Soc. **34**, 150 (1999).
[3] S. Takamiya, M. Harayama, T. Sugimura and S. Hashimoto, Solid-State Electron. **42**, 447 (1998).
[4] G. Meneghesso, A. Neviani, R. Oesterholt and E. Zanoni, IEEE Trans. Electron Dev. **46**, 2 (1999).
[5] R. Menozzi, Semicond. Sci. Technol. **13**, 1053 (1998).
[6] G. Meneghesso, E. D. Bortoli, D. Sala and E. Zanoni, Microelectron. Reliability **37**, 1121 (1997).

[7] J. Laskar, J. M. Bigelow and J. Kolodzey, IEEE Trans. Electron Dev. **39**, 257 (1992).
[8] N. Labat, N. Saysset, A. Touboul, Y. Danto and F. Fantini, Microelectron. Reliability **37**, 1675 (1997).
[9] Y. C. Chou, G. P. Li, Y. C. Chen and T. A. Midford, IEEE Electron Dev. Lett. **18**, 479 (1996).
[10] M. H. Somerville, J. A. Alamo and P. Saunier, IEEE Trans. Electron Dev. **45**, 1883 (1998).
[11] J. P. Sun, G. I. Haddad, P. Mazumder and J. N. Schulman, Proceedings of the IEEE **86**, 641 (1998).
[12] C.-L. Wu and W. C. Hsu, IEEE Trans. Electron Dev. **43**, 207 (1996).
[13] M. Keever, K. Hess and M. Ludowise, IEEE Electron Dev. Lett. **3**, 297 (1982).
[14] J.-P. Leburton and J. Kolodzey, IEEE Trans. Electron Dev. **35**, 1530 (1988).